



HAL
open science

Testing the genetic relationship between fluid alteration and brecciation in CM chondrites

Maximilien Verdier-paoletti, Yves Marrocchi, Lionel Vacher, Jérôme Gattacceca, Andrey Gurenko, Corinne Sonzogni, Matthieu Gounelle

► To cite this version:

Maximilien Verdier-paoletti, Yves Marrocchi, Lionel Vacher, Jérôme Gattacceca, Andrey Gurenko, et al.. Testing the genetic relationship between fluid alteration and brecciation in CM chondrites. *Meteoritics and Planetary Science*, 2019, 54 (8), pp.1692-1709. 10.1111/maps.13306 . hal-02275843

HAL Id: hal-02275843

<https://hal.science/hal-02275843v1>

Submitted on 15 Nov 2024





HAL is a multi-disciplinary open access archive for the deposit and dissemination of scientific research documents, whether they are published or not. The documents may come from teaching and research institutions in France or abroad, or from public or private research centers.

L'archive ouverte pluridisciplinaire **HAL**, est destinée au dépôt et à la diffusion de documents scientifiques de niveau recherche, publiés ou non, émanant des établissements d'enseignement et de recherche français ou étrangers, des laboratoires publics ou privés.



Distributed under a Creative Commons Attribution 4.0 International License

Testing the genetic relationship between fluid alteration and brecciation in CM chondrites

Maximilien J. VERDIER-PAOLETTI ^{1,2*}, Yves MARROCCHI³, Lionel G. VACHER ^{3,4},
Jérôme GATTACCECA ⁵, Andrey GURENKO³, Corinne SONZOGNI⁵, and
Matthieu GOUNELLE ^{1,6}

¹IMPMC, MNHN, UPMC, UMR CNRS 7590, 61 rue Buffon, 75005 Paris, France

²Department of Terrestrial Magnetism, Carnegie Institution of Washington, Washington, District of Columbia 20015, USA

³CRPG, CNRS, Université de Lorraine, UMR 7358, Vandoeuvre les Nancy F-54501, France

⁴Department of Physics, Washington University, St. Louis, St. Louis, Missouri 63130, USA

⁵CNRS, Aix-Marseille Univ, IRD, Coll France, CEREGE, Aix-en-Provence, France

⁶Institut Universitaire de France, Maison des Universités, 103 bd. Saint-Michel, 75005 Paris, France

*Corresponding author. E-mail: mverdier@carnegiescience.edu

(Received 10 October 2018; revision accepted 27 April 2019)

Abstract—Boriskino is a poorly studied CM chondrite with numerous millimeter- to centimeter-scale clasts exhibiting sharp boundaries. Clast textures and mineralogies attest to diverse geological histories with various degrees of aqueous alteration. We conducted a petrographic, chemical, and isotopic study on each clast type of the breccia to investigate if there exists a genetic link between brecciation and aqueous alteration, and to determine the controlling parameter of the extent of alteration. Boriskino is dominated by CM2 clasts for which no specific petrographic type could be assigned based on the chemical compositions and modal abundances of constituents. One clast stands out and is identified as a CM1 lithology, owing to its lack of anhydrous silicates and its overall abundance of dolomite-like carbonates and acicular iron sulfides. We observe that alteration phases near clast boundaries exhibit foliation features, suggesting that brecciation postdated aqueous alteration. We measured the O-isotopic composition of Ca-carbonates and dolomite-like carbonates to determine their precipitation temperatures following the methodology of Verdier-Paoletti et al. (2017). Both types of carbonates yield similar ranges of precipitation temperatures independent of clast lithology, ranging from -13.9 ± 22.4 (2σ) to 166.5 ± 47.3 °C, precluding that temperature alone accounts for the differences between the CM1 and CM2 lithologies. Instead, we suggest that initial water/rock ratios of 0.75 and 0.61 for the CM1 and CM2 clasts, respectively, might control the extent of aqueous alteration. Based on these estimates, we suggest that Boriskino clasts originated from a single parent body with heterogeneous distribution of water either due to local differences in the material permeability or in the initial content of ice available. These conditions would have produced microenvironments with differing geochemical conditions thus leading to a range of degrees of aqueous alteration.

INTRODUCTION

Mighei-like chondrites (CM) represent 25% of carbonaceous chondrite falls. Their infrared spectra link them to the remnants of the early solar system (primitive C-complex and C asteroids; Burbine 2014) making CM chondrites a valuable source of information

for deciphering the prevailing conditions of the early solar system. CM-like matter also represents a significant fraction of exogenic clasts in other groups of meteorites, suggesting that their parent bodies are widespread in the asteroid belt (Zolensky et al. 1997; Gounelle et al. 2005; Bischoff et al. 2006; Briani et al. 2012). To a few exceptions, like the Y-791198 and Paris

meteorites (Chizmadia and Brearley 2008; Hewins et al. 2014; Vacher et al. 2016), all CM chondrites are described as impact/regolith breccias (Bischoff et al. 2006), as they contain solar-wind–implanted rare gases and have clastic matrices consistent with a near-surface origin on their parent body (Greenwood et al. 1993; Nakamura et al. 1999; Bekaert et al. 2019). Although they are categorized as lightly shocked (Scott et al. 1992), their chondrules, isolated anhydrous minerals, and matrix phyllosilicates often display foliation features consistent with multiple hypervelocity impacts (Rubin 2012; Hanna et al. 2015; Lindgren et al. 2015; Vacher et al. 2018). CM chondrites thus recorded the postaccretion evolution of asteroids and enabled regolith gardening to be studied in detail.

CM chondrites are characterized by complex assemblages of constituents formed at high temperatures (chondrules, Fe-Ni metal beads, and rare amoeboid-olivine-aggregates [AOAs] and Ca-Al-rich inclusions [CAI]) that most likely originated in the protoplanetary disk, and secondary minerals (e.g., oxides, sulfides, phyllosilicates, and carbonates) that formed during subsequent oxidation events. Hydrous phases are mostly considered to result from multiple aqueous alteration events in the CM asteroidal parent bodies (e.g., McSween 1979a; Tomeoka and Buseck 1985; Benedix et al. 2003), although some authors have suggested that hydration could have occurred on a previous uncompact parent body (Metzler et al. 1992), or that a small fraction of the phyllosilicates might have formed in the protoplanetary disk (Ciesla et al. 2003).

Aqueous alteration has been extensively studied in CM chondrites (e.g., McSween 1979a; Benedix et al. 2003; Rubin et al. 2007; Lee et al. 2014; Pignatelli et al. 2016, 2017, 2018; Van Kooten et al. 2018), and oxygen isotopes are a powerful tool for constraining the physicochemical conditions (T , W/R , pH, etc.) and relative timing of secondary phase precipitation. Among secondary phases, meteoritic carbonates represent the direct snapshots of the isotopic compositions of alteration fluids and can thus be used to characterize the isotopic evolution of the CM parent bodies (Benedix et al. 2003; Tyra et al. 2012; Fujiya et al. 2015; Vacher et al. 2016, 2017; Lindgren et al. 2017; Marrocchi et al. 2018). Recent studies have revealed that the O-isotopic compositions of CM carbonates define a continuous trend (slope ≈ 0.65) that is indistinguishable within error from that defined by both the bulk and matrix phyllosilicates (Verdier-Paoletti et al. 2017). This implies that (1) isotopic equilibrium between $^{17,18}\text{O}$ -rich fluid and ^{16}O -rich anhydrous silicates controlled the O-isotopic evolution of CM chondrites at both the bulk and mineral scales (Clayton and Mayeda 1984, 1999; Verdier-Paoletti et al. 2017) and (2) CM chondrites

accreted anhydrous silicates and water ice grains characterized by two distinct but homogeneous initial O-isotopic compositions. The O-isotopic compositions of carbonates can thus be used to better understand the physicochemical parameters that controlled the varying degrees of alteration observed within a given CM chondrite. It should be kept in mind that alternative models considering fluid flow over km scales have been invoked to explain the variations in the degree of alteration and O-isotopic composition within chondrite groups (Young et al. 1999, 2003). However, no evidence of large-scale fluid flow has been described to date.

It has been suggested that impacts might locally induce and/or intensify secondary processes on the asteroidal parent body (Davidson et al. 2012; Rubin 2012; Lindgren et al. 2015). Although alteration has been shown to clearly predate brecciation in a few cases (Metzler et al. 1992), in this context, assessing whether these disruptive events occurred prior, concomitantly, or after aqueous alteration is difficult to decipher. The previous extensive petrographic study of the clast-bearing meteorite LON 94101 conducted by Lindgren et al. (2013) concluded for alteration occurring mainly before the accretion of debris. However, the mineralogical and textural diversity of clasts within this meteorite has been considered as evidence for a diversity of sources. Indeed, some CM chondrites are polymict breccias (i.e., clasts of different chondritic groups), leading to important difficulties in unraveling the geological history of the initial parent body.

Here, we report a petrographic, mineralogical, and isotopic survey of the genomict CM breccia Boriskino (Fig. 1). This chondrite fell in the early afternoon on April 20, 1930 near the village of Staroe Boriskino (Russia). Two stones with a total weight of 1.34 kg were collected (Mason 1963). Boriskino was first described as a moderately hydrated type II chondrite (Wiik 1956) before reclassification as a CM chondrite (Wasson 1974). However, Boriskino comprises several lithologies that differ in texture and mineralogy attesting to different geological histories comparable to what has been reported in the Murray meteorite (Rubin and Wasson 1986). Boriskino may thus provide a better understanding of the variability in secondary processes experienced by CM chondrites and the potential genetic relationship between fluid alteration and brecciation in establishing their petrographic, chemical, and isotopic characteristics.

MATERIALS AND METHODS

Two thick sections of the Boriskino meteorite, named 3788-1 and 3788-2, embedded in epoxy resin, were loaned by the Muséum National d'Histoire

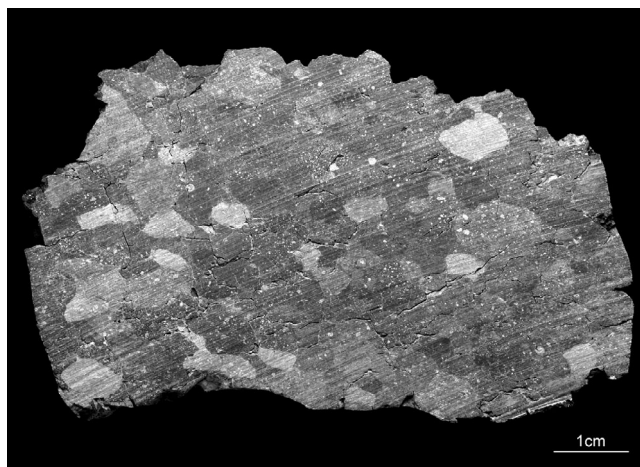


Fig. 1. Reflected light photograph of a piece of the Boriskino CM chondrite, courtesy of L. D. Bayle. Diverse lithologies, characterized by different shades of gray, can be distinguished. Saw marks are still visible in the cut face.

Naturelle of Paris. Backscattered electron (BSE) images and X-ray elemental distribution maps were acquired at the Muséum National d'Histoire Naturelle (Paris) using a TESCAN Vega 2LSU scanning electron microscope with an accelerating voltage of 15 kV. Samples were coated with a carbon layer of 18–20 nm thickness to avoid charging effects. To distinguish as many phases as possible, we generated composite elemental maps using ImageJ software. Lithology boundaries were visually determined from reflected light and BSE observations based on the matrix hue, boundary sharpness, and texture of major opaque constituents. Constituent modal abundances were determined via point counting using JMicroVision software. Approximately 1000 points were acquired on X-ray composite maps in each lithology of sections 3788-1 and 3788-2 to attain a sufficient binomial confidence interval for our estimates (Van der Plas and Tobi 1965). Matrix and chondrule modal abundances were determined by counting approximately 300 points over BSE mosaics, enabling a better discrimination between these phases (Table 1).

Quantitative compositional analyses were performed using a CAMECA SX-Five electron microprobe at the CAMPARIS facility, University of Paris VI (France). All measurements were performed with an accelerating voltage of 15 keV and a beam current of 10 nA. The beam diameter was set to ~5 μm for sulfide, metal, carbonate, and tochilinite–cronstedtite intergrowth (TCI) analyses, and was defocused to ~10 μm for the matrix. The following standards were used for sulfides and metal: diopside for Si, pyrite for S and Fe, pure cobalt for Co, and NiO for Ni. Typical detection limits were 0.10 atom% for Si, 0.26 atom% for S, 0.24

atom% for Fe, 0.22 atom% for Co, and 0.18 atom% for Ni. Each measurement exhibiting a Si concentration above 1 atom% was excluded. Standards for TCI, carbonate, and matrix analyses were: albite for Na; diopside for Mg, Si, and Ca; orthoclase for Al and K; apatite for P; pyrite for S; Cr_2O_3 for Cr; MnTiO_3 for Mn; Fe_2O_3 for Fe; NiO for Ni; and SrSi for Sr. Typical detection limits were 0.05 wt% for Na and Mg; 0.04 wt% for P and Ca; 0.06 wt% for Si, Al, S, and K; 0.08 wt% for Cr; 0.09 wt% for Mn; 0.13 wt% for Fe and Ni; and 0.18 wt% for Sr. Carbonates with Si or S contents above 1 mole% were excluded as the measurement was considered to be contaminated by adjacent material. As in Pignatelli et al. (2016), TCIs with S > 10 wt% and Si < 5 wt% were considered tochilinite, those with Si > 7 wt% and S < 5 wt% were regarded as cronstedtite, and others were assigned as intermediate.

Bulk oxygen isotopic measurements were conducted at the Stable Isotopes Laboratory of CEREGE (Aix-en-Provence, France). Twenty milligrams of Boriskino were ground using an agate mortar. Three aliquots (2 mg) obtained from the fraction of 200–400 μm were exposed to 150 mbar of gaseous bromine pentafluoride (BrF_5) to break SiO_2 bonds and were irradiated with a 30 W CO_2 infrared laser to catalyze the reaction. Emitted gas was purified through three liquid N traps and one heated solid KBr trap before reaching the molecular oxygen trap (frozen with liquid N for 10 min). The molecular oxygen trap was then heated to near 100 $^\circ\text{C}$ to release the adsorbed molecules, which were conveyed for 5 min to an ethanol + liquid N slush at roughly -119 $^\circ\text{C}$ for condensation of NF_3 molecules which might interfere with ^{17}O measurements. The molecular trap was then refrozen for 5 min and reheated to release newly adsorbed O_2 molecules to the dual-inlet ThermoFinnigan DeltaPlus mass spectrometer. The sample and reference gases were alternatively measured eight times each. Oxygen isotope measurements are expressed in ‰ referenced against the V-SMOW standard as: $\delta^{18}\text{O} = ([^{18}\text{O}/^{16}\text{O}]_{\text{sample}}/[^{18}\text{O}/^{16}\text{O}]_{\text{standard}} - 1) \times 1000$ and $\delta^{17}\text{O} = ([^{17}\text{O}/^{16}\text{O}]_{\text{sample}}/[^{17}\text{O}/^{16}\text{O}]_{\text{standard}} - 1) \times 1000$. The $\delta^{17,18}\text{O}$ values of the reference gas were fixed through the measurement of standard NBS28 ($\delta^{18}\text{O} = 9.60$ ‰; Gröning 2004), fabricated to have an O-isotopic composition related by mass-dependent fractionation to V-SMOW. Mass-dependent fractionations are described by the terrestrial fractionation line (TFL; slope 0.52 on the three O-isotope plot), whereas mass-independent fractionations are represented by $\Delta^{17}\text{O} = \delta^{17}\text{O} - 0.52 \times \delta^{18}\text{O}$. Measurements were corrected on a daily basis using 1.5 mg internal quartz standards. Analytical uncertainties derived from repeated measurement of this internal standard are 0.08, 0.12, and 0.03‰ for $\delta^{17}\text{O}$, $\delta^{18}\text{O}$, and $\Delta^{17}\text{O}$, respectively.

Table 1. Modal abundances (vol%) of the constituents and petrographic characteristics in sections 3788-1 and 3788-2 with 2σ errors in brackets.

	Lithology A		Lithology B		Lithology C		Lithology D		Lithology E	
	Section 1	Section 2	Section 1	Section 2	Section 1	Section 2	Section 1	Section 2	Section 1	Section 2
Dark matrix*	42.1 (5.7)	44.4 (5.7)	43.4 (5.7)	45.3 (5.7)	43.4 (5.7)	44.2 (5.7)	70.0 (2.9)	74.9 (5.0)	47.2 (5.7)	44.9 (5.7)
Light matrix*	37.2 (5.5)	37.2 (5.5)	25.7 (5.0)	28.3 (5.2)	40.1 (5.6)	43.6 (5.7)	Absent	Absent	40.3 (5.6)	41.6 (5.6)
Chondrules*	11.2 (3.6)	11.5 (3.7)	10.5 (3.5)	11.3 (3.6)	11.3 (3.6)	7.6 (3.0)	16.5 (2.3)	7.6 (3.0)	5.3 (2.6)	5.3 (2.6)
Carbonates	4.2 (1.3)	6.1 (1.5)	3.9 (1.2)	2.8 (1.0)	10.0 (1.9)	7.1 (1.6)	13.1 (2.1)	7.5 (1.7)	2.5 (1.0)	2.2 (0.9)
CAIs	0.3 (0.3)	Absent	0.1 (0.2)	Absent	0.9 (0.6)	0.7 (0.5)	0.1 (0.2)	Absent	0.3 (0.3)	0.1 (0.2)
Metal	0.1 (0.2)	Absent	0.1 (0.2)	Absent	0.7 (0.5)	0.2 (0.3)	3.1 (1.1)	0.1 (0.2)	0.5 (0.4)	0.1 (0.2)
Sulfides	7.2 (1.6)	5.0 (1.4)	8.5 (1.8)	9.6 (1.9)	2.5 (1.0)	0.6 (0.5)	3.7 (1.2)	0.7 (0.5)	6.2 (1.5)	7.8 (1.7)
Chondrule mesostasis	Phyllosilicates	Phyllosilicates	Phyllosilicates	Phyllosilicates	Phyllosilicates	Phyllosilicates	Phyllosilicates	Phyllosilicates	Phyllosilicates	Phyllosilicates
Silicates in chondrules	Partially altered	Partially altered	Phyllosilicates	Phyllosilicates	Partially altered	Partially altered	Partially altered	Partially altered	Partially altered	Partially altered
Points	1013	1005	1005	1010	1014	1027	1008	1010	1010	1008
Surface (mm ²)	11.8	33.4	25.0	27.2	15.8	39.5	7.1	6.3	6.5	13.6

*Modal abundances acquired over a BSE mosaic map with approximately 300 points; as a consequence, totals do not equal 100%.

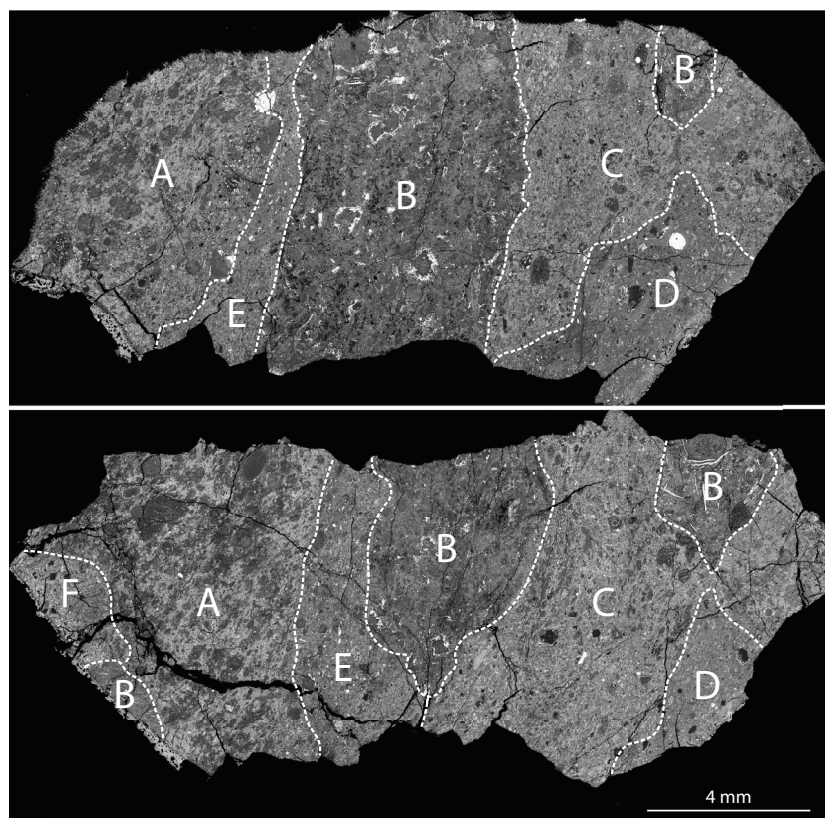


Fig. 2. BSE images of Boriskino sections 3788-1 (top) and 3788-2 (bottom). Dashed white lines represent lithology boundaries considered in this study. Lithology B is encountered in the middle and upper right parts of both sections.

In situ oxygen isotopic measurements were performed during two sessions at CRPG-CNRS (Nancy, France) using a Cameca IMS 1280HR following the procedure of Rollion-Bard and Marin-Carbonne (2011). We used a Cs^+ primary ion beam (15 keV, ~ 7 nA) and an electron flow parallel to the sample surface to neutralize charge excesses. $^{16}\text{O}^-$, $^{17}\text{O}^-$, and $^{18}\text{O}^-$ ions were counted in multicollection mode using three Faraday cups. Each measurement was corrected for instrumental mass fractionation determined by replicate analyses of four terrestrial standards: San Carlos olivine, quartz, magnetite, and Mexico calcite. No distinction was made for our Ca-carbonates between the calcite and aragonite polymorphs. However, it was reported that, even at low temperature, fractionation in the aragonite–calcite system is expected to be negligible (i.e., at 0°C $\alpha_{\text{aragonite-calcite}} \approx 1\text{--}2\text{‰}$; Chacko and Deines 2008). Regarding dolomite analyses, it is known that MgO, FeO, and MnO contents affect the yields of O-isotopes in Mg-rich carbonates (Rollion-Bard and Marin-Carbonne 2011). Considering this matrix effect, we added the DPA ankerite to our suite of standards, as its chemical composition is closer to the average of our dolomites than the Nepal dolomite standard (see Fig. 9 and

Table 3). We were not able to reproduce the calibration trends observed in Rollion-Bard and Marin-Carbonne (2011) as we did not consider as many carbonates standards. However, assuming similar trends, the dispersion in MgO and FeO + MnO contents in our dolomite relative to DPA would lead to minimal matrix effects between -0.4 and -1.2‰ . The O-isotopic ratios of Ca-carbonates were normalized to that of the terrestrial calcite standard while those of dolomites are normalized to DPA; all are expressed in delta notation. The 2σ errors were $0.3\text{--}0.6\text{‰}$ for $\delta^{17}\text{O}$, $0.2\text{--}1.1\text{‰}$ for $\delta^{18}\text{O}$, and $0.1\text{--}0.6\text{‰}$ for $\Delta^{17}\text{O}$. The error on $\Delta^{17}\text{O}$ was calculated by propagating the errors on $\delta^{17}\text{O}$ and $\delta^{18}\text{O}$, and the SD of $\Delta^{17}\text{O}$ values of the calcite or ankerite terrestrial standards. After the SIMS measurement session, all analytical spots were observed using secondary electron microscopy to verify that the beam did not overlap onto the matrix or any adjacent silicate; any measurements affected by beam overlap were rejected.

RESULTS

Boriskino comprises centimeter-sized irregular clasts visible to the naked eye with well-defined boundaries comparable to what has been reported for

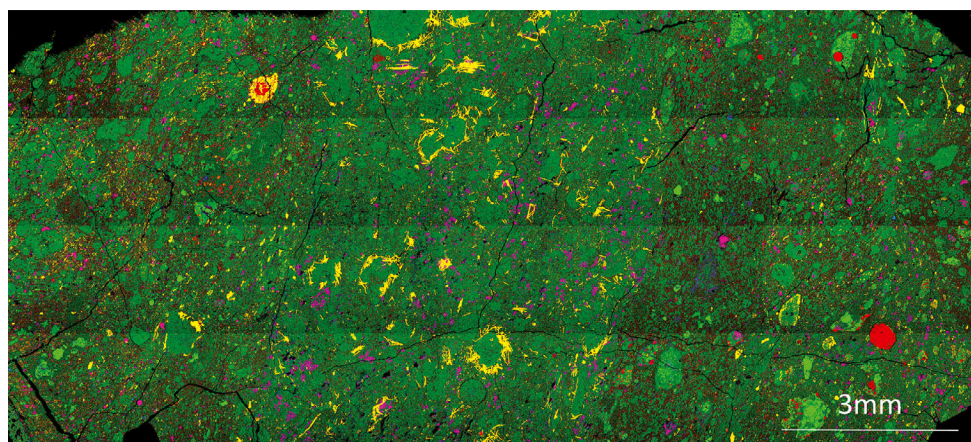


Fig. 3. Composite X-ray elemental map of Boriskino section 3788-1. Colors are Fe (red), Mg (green), Al (blue), Ca (magenta), and S (yellow) to enable distinction of carbonates (magenta), sulfides (yellow-orange), CAIs (purple-blue), metal (red), and silicates (green). (Color figure can be viewed at wileyonlinelibrary.com.)

Nogoya (Heymann and Mazor 1967); each clast is characterized by a different shade of gray in reflected light, and some host white opaque phase inclusions (Fig. 1). Several centimeter-long fractures cross multiple clasts (Fig. 1).

Within two sections, we determined six different lithologies that we refer to as A–F (Figs. 2 and 3). Lithology F is relatively small (approximate size 3×2 mm) and will thus not be considered further. Lithologies A, B, and C are the most abundant,

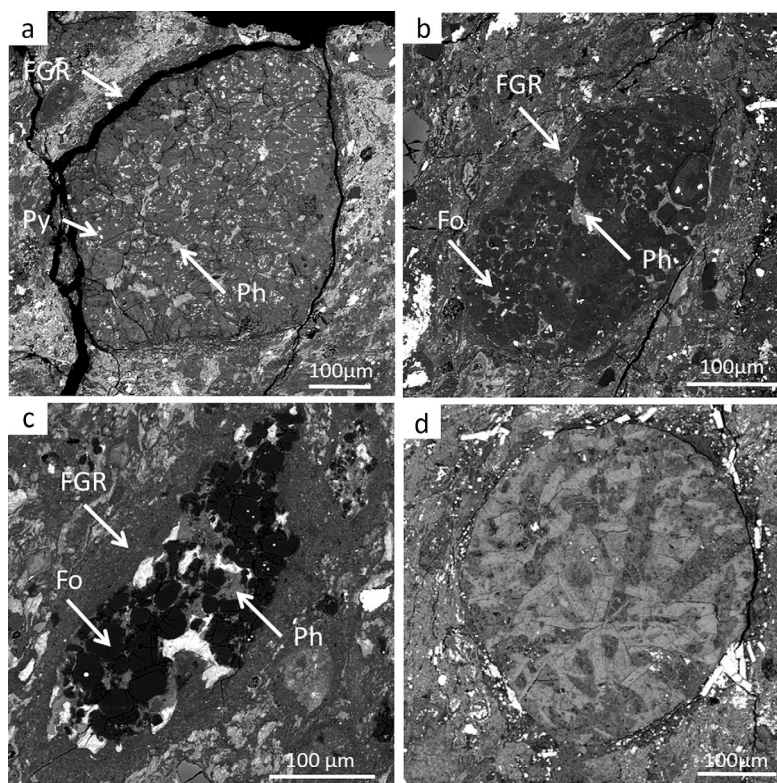


Fig. 4. a–c) Type I chondrules in section 3788-2 from lithologies A, E, and C, respectively. Mesostasis has been replaced by phyllosilicates (Ph), and fine-grained rims (FGR) are always present. Pyrrhotite (Py) inclusions in forsterite (Fo) are abundant. d) Pseudomorphosed radial chondrule in lithology B. Anhydrous minerals have been completely pseudomorphosed by phyllosilicates and are often surrounded by acicular sulfides.

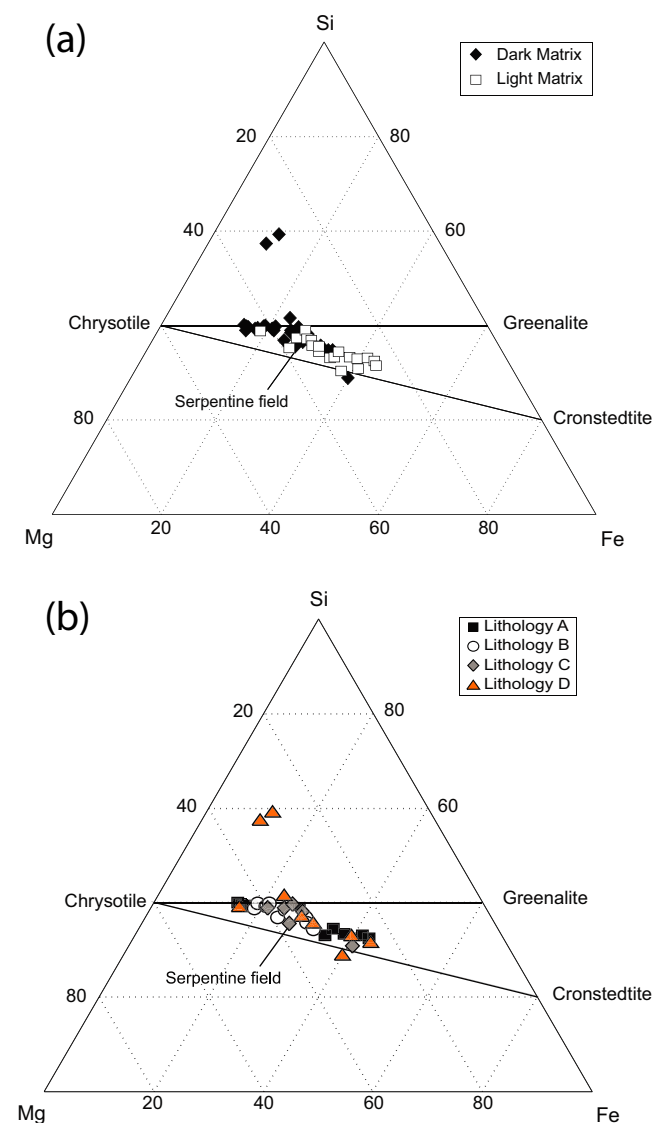


Fig. 5. Mg-Si-Fe ternary diagrams of matrix analyses (atom%). Both diagrams display the serpentine field delimited by the elemental ratios for stoichiometric chrysotile, greenalite, and cronstedtite. a) “Bright matrix” refers to fine-grained material appearing bright in BSE SEM observations due to higher concentrations in iron compared to “dark matrix” material that is richer in magnesium and thus represents by-products of higher extents of aqueous alteration (McSween 1979b). b) Matrix chemical compositions displayed based on the host lithology. No significant chemical differences are apparent between matrix lithologies. (Color figure can be viewed at wileyonlinelibrary.com.)

representing 24.3, 28.0, and 29.7% of the total surface of the two sections. All lithologies (A–E) show significant alteration, with the complete replacement of glassy chondrule mesostases by phyllosilicates (Fig. 4) and an absence of Fe-Ni metal beads (Table 1). Chondrules of lithology B are pseudomorphed by phyllosilicates and are

surrounded by acicular sulfides (Fig. 4d). Fine-grained rims are always observed around chondrules (Fig. 4). Reflected light and mean atomic number contrast BSE imaging maps reveal two types of matrices present in each lithology (1) a bright matrix mainly composed of phyllosilicates and (2) a dark matrix of brown structures that resemble pseudomorphosed chondrules. The modal abundance of the dark matrix is higher in all lithologies except lithology C, where both matrices are present in the same proportions. Both types of matrices have similar chemical compositions that fall in the serpentine field (Fig. 5; Table S1 in supporting information), except two regions that show compositions close to saponite. Phyllosilicates and chondrules located at lithological boundaries exhibit foliation features (Fig. 6). Anhydrous silicates in the boundary regions have fractures perpendicular to the foliation plane (Fig. 6c).

Iron sulfides are ubiquitous in Boriskino (Fig. 7) (Table 2). In lithology B, acicular sulfides up to 600 μm long (chemical composition close to mackinawite $[(\text{Fe}_{1.025 \pm 0.052}\text{Ni}_{0.012 \pm 0.005})_{1.037}\text{S}]$) surround pseudomorphosed chondrules. In other lithologies, sulfides are present as irregular and/or euhedral grains 30–200 μm in size, with chemical compositions close to troilite $[(\text{Fe}_{0.991 \pm 0.053}\text{Ni}_{0.082 \pm 0.005}\text{Co}_{0.003})_{1.076}\text{S}]$. Two troilite crystals containing exsolved pentlandite $[(\text{Fe}_{0.655 \pm 0.043}\text{Ni}_{0.586 \pm 0.050}\text{Co}_{0.025 \pm 0.007})_{1.266}\text{S}]$ were observed in lithology C.

Tochilinite–cronstedtite intergrowths are absent from lithologies B and D, but occur in other lithologies as type II TCI clumps of several hundred square micrometers in size. Although most TCIs occur as irregular anhedral or subhedral grains 30–40 μm in size, some are euhedral, characteristic of anhydrous silicate pseudomorphism (Pignatelli et al. 2016). In section 3788-1, we performed 190 microprobe measurements over 40 dispersed TCIs: 28 ($n = 142$) in lithology A and 12 ($n = 48$) in lithology C. Following the criteria defined by Pignatelli et al. (2016), 145 of those measurements were considered as cronstedtite, 39 were undetermined, and only two occurrences of tochilinite were observed in lithology A. All TCIs of lithology A span a wide range of compositions ($\text{FeO}/\text{SiO}_2 = 1.56 \pm 1.28 [2\sigma]$ and $\text{S}/\text{SiO}_2 = 0.2 \pm 0.3$) compared to lithology C ($\text{FeO}/\text{SiO}_2 = 1.09 \pm 0.64$ and $\text{S}/\text{SiO}_2 = 0.11 \pm 0.13$). Thirteen TCIs scattered in section 3788-2 were considered: one in A ($n = 7$), seven in C ($n = 43$), and five in E ($n = 25$). One measurement in lithology C yields a composition akin to tochilinite; approximately half of the remaining measurements have compositions close to cronstedtite ($n = 38$), and the other half correspond to a mixture between cronstedtite and tochilinite ($n = 36$). FeO/SiO_2 and S/SiO_2 ratios of TCIs of the same lithologies are significantly different from one section to the other, with

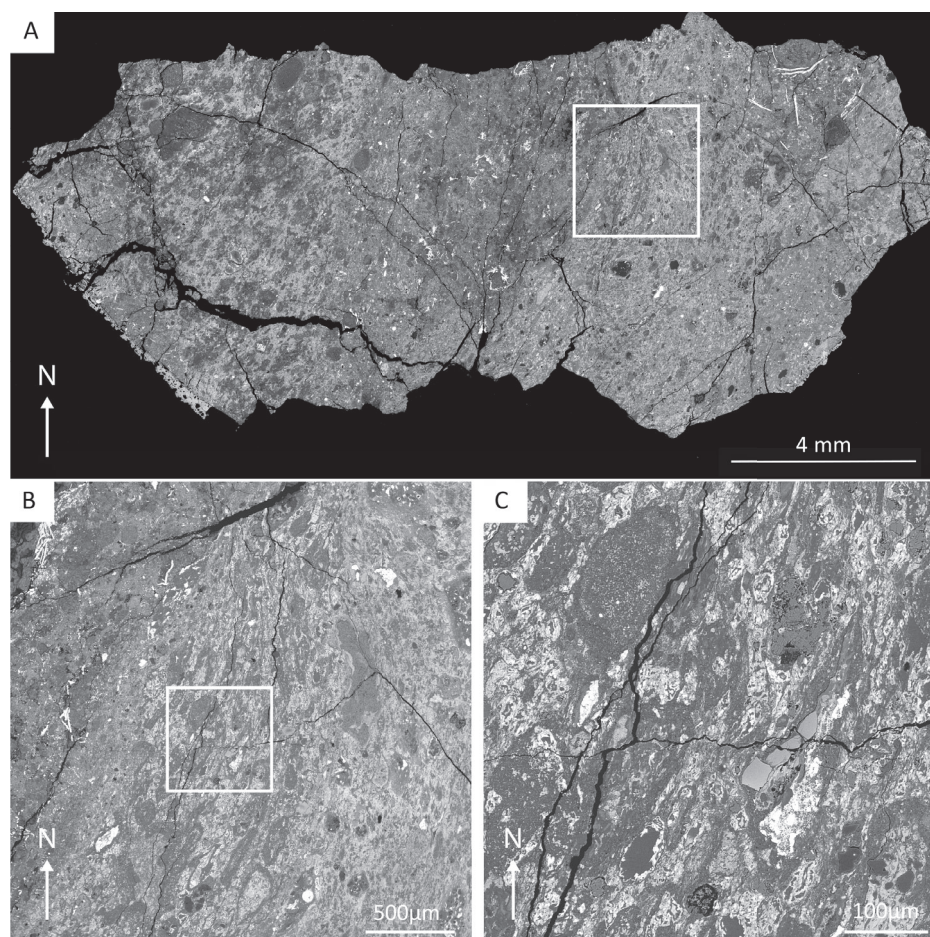


Fig. 6. a) BSE mosaic of Boriskino section 3788-2. The white square delimits the magnified region in (b). b) BSE image of a region close to the central lithology. Phyllosilicates and chondrules are flattened in a preferential NW-SE direction. The white square delimits the magnified region in (c). c) Fractures are ubiquitous in the meteorite, especially close to lithology boundaries. Anhydrous minerals in those regions frequently exhibit fractures oriented almost perpendicular to the foliation plane.

FeO/SiO₂ and S/SiO₂ in section 3788-2 of: 3.13 ± 1.23 and 0.41 ± 0.25 respectively in lithology A, and 2.14 ± 1.03 and 0.34 ± 0.27 in lithology C. TCIs in lithology E yield FeO/SiO₂ = 1.62 ± 0.67 and S/SiO₂ = 0.14 ± 0.16 .

The bulk oxygen isotope compositions of the three aliquots from Boriskino are $\delta^{18}\text{O} = 7.50, 8.73,$ and 9.03‰ and $\delta^{17}\text{O} = 1.70, 3.07,$ and 2.27‰ . These results fall along the CM trend in a three-isotope plot with $\Delta^{17}\text{O} = -2.20, -1.46,$ and -2.43‰ (Fig. 8). This result strengthens the inferred CM nature of Boriskino as it is the first measurement of its bulk oxygen isotopic composition.

Carbonates are ubiquitous in Boriskino (Fig. 3; Table 1). A total of 18 carbonates were considered across both sections, distributed across five lithologies: A ($n = 3$), B ($n = 10$), C ($n = 2$), E ($n = 1$), and F ($n = 2$). Most Ca-carbonates are 40–60 μm long and almost always have important fractures. A few

subhedral grains partially pseudomorphized by TCIs were observed. However, most Ca-carbonates are anhedral, containing Fe-Ni sulfides and micropores, corresponding to type 2a calcite (Tyra et al. 2012; Lee et al. 2014; Vacher et al. 2017). Ca-carbonates have compositions of 96.5–100.3 wt% CaCO₃ with Ca contents between 96.5 and 99.6 mole% (Fig. 9; Table 3). The remaining fraction of carbonates has compositions consistent with ankerite of the dolomite group and will be referred to as “dolomite” hereafter. They have compositions spanning from 49.3 to 54.8 and 32.7 to 37.3 wt% of CaCO₃ and MgCO₃, respectively, with Ca and Mg contents of 48.3–53.8 and 38.2–42.8 mole%, respectively, and Fe+Mn content ranging from 7.2 to 11.4 mole%. In both sections, dolomite carbonates were systematically present in lithology B, with one exception in lithology C. They occur as irregular subhedral polycrystalline grains up to 200 μm long and are often associated with acicular sulfides.

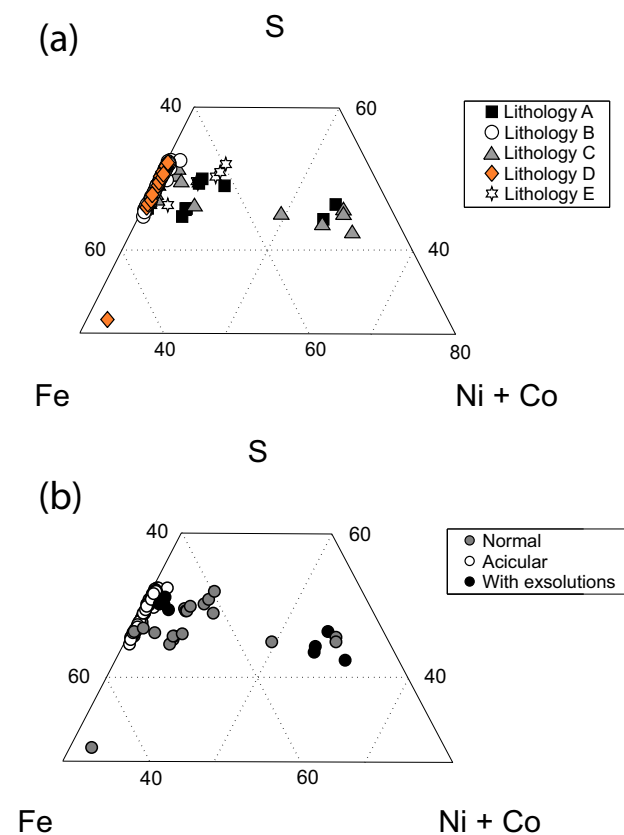


Fig. 7. Cropped Fe-S-(Ni+Co) ternary diagrams of sulfide compositions (atom%) relative to (a) their morphologies and (b) their host lithology. Exsolved minerals are systematically Ni-rich and are absent in acicular sulfides at the micron scale. (Color figure can be viewed at wileyonlinelibrary.com.)

We compiled our measurements of the O-isotopic compositions of carbonates in the section 3788-1 of Boriskino with those already reported for sections 3788-3 and -4 from Vacher et al. (2018). The lithology 1 reported in their study corresponds to our lithology A, while others exhibit textures and abundances of major constituents that differ from the ones in our study. As a consequence, those lithologies are hereafter labeled as “undetermined.” Boriskino Ca-carbonates have $\delta^{18}\text{O}$ values ranging from 14.7 ± 0.8 (2σ) to $38.4 \pm 0.9\text{‰}$, $\delta^{17}\text{O}$ from 4.8 ± 0.6 to $20.0 \pm 0.6\text{‰}$, and $\Delta^{17}\text{O}$ from -3.5 ± 0.4 to $0.0 \pm 0.3\text{‰}$ (Fig. 10a; Table 4). They define a discontinuous trend with two distinct populations, characterized by average O-isotopic compositions of $\delta^{18}\text{O} = 18.8 \pm 0.9\text{‰}$ and $\delta^{17}\text{O} = 7.3 \pm 0.5\text{‰}$ ($n = 16$, errors are 2s.e.) and $\delta^{18}\text{O} = 34.0 \pm 1.4\text{‰}$ and $\delta^{17}\text{O} = 16.9 \pm 0.8\text{‰}$ ($n = 13$). Dolomites in section 3788-1 have the lightest O-isotopic compositions with $\delta^{18}\text{O}$ values from 12.7 ± 0.4 to $17.5 \pm 0.4\text{‰}$ and $\delta^{17}\text{O}$ from 4.0 ± 0.6 to $5.2 \pm 0.5\text{‰}$ and $\Delta^{17}\text{O}$ from -4.3 ± 0.4 to $-2.1 \pm 0.4\text{‰}$ (Fig. 10a; Table 5).

DISCUSSION

Macro and Micro Brecciation

Macroscopic observations of Boriskino highlight the brecciated nature of CM chondrites, with clasts larger than 1 cm (Fig. 1). Petrographic studies of chondrites, however, are typically performed on subcentimeter-size sections (often single clasts of a breccia), possibly introducing bias in our interpretations. This property also demonstrates the difficulty of classifying CM chondrites on the basis of micrometric mineralogical indexes such as TCI chemical compositions (Rubin et al. 2007), especially considering their chemical zoning (Pignatelli et al. 2016). Therefore, assessment of the global history of CM chondrites requires observations at the macroscopic scale in addition to classical microscopic characterization. Brecciation features are difficult to interpret, but could result from accretion of debris during disruptive collisions between asteroids (Bischoff et al. 2006). However, the diversity of clasts constituting Boriskino can either come from (1) the accretion of debris from multiple parent bodies with different geological histories (e.g., Zolensky et al. 1996; Lindgren et al. 2013) or (2) fragments of a single parent body in which alteration occurred in multiple microenvironments with different geochemical conditions (T and/or water/rock ratio; e.g., Brearley 2006; Palmer and Lauretta 2011).

It was recently shown that the O-isotopic compositional variations in Ca-carbonates in CM chondrites define the continuous trend $\delta^{17}\text{O} = (0.66 \pm 0.05 \times \delta^{18}\text{O}) - 4.7 \pm 1.5$ (2σ , $R^2 = 0.87$, MSWD = 3.3; Verdier-Paoletti et al. 2017). This trend is parallel to that defined by the inferred O-isotopic compositions of water in different CM chondrites (CM water; hereafter CMW). The difference in intercept between both trends is directly related to the temperature of carbonate precipitation, proposed to be 113 ± 54 °C on average (Verdier-Paoletti et al. 2017). Ca-carbonates hosted in the different lithologies of Boriskino also define a global trend of $\delta^{17}\text{O} = (0.63 \pm 0.001 \times \delta^{18}\text{O}) - 4.30 \pm 0.03$ (2σ , $R^2 = 0.98$, MSWD = 1.2), similar within errors to that defined by nine different CM chondrites (Verdier-Paoletti et al. 2017). This similarity implies that all Ca-carbonates precipitated from fluids that followed the same isotopic evolution and experienced the same narrow range of temperatures. Such conditions could be achieved within a single parent body characterized by relatively small spatial variations in geochemical conditions. However, we cannot exclude that such O-isotopic characteristics could have been established in different parent bodies, although this would imply that they accreted anhydrous silicates and water from the same respective isotopically homogeneous reservoirs; otherwise, different relationships

Table 2. Representative chemical compositions (atom%) of sulfides in sections 3788-1 and 3788-2. Sulfides were characterized following the procedure of Rubin et al. (2007) based on Ni/(Ni + Fe) ratio: 0–0.1 = Pyrrhotite, 0.1–0.4 = Intermediate, >0.4 = Pentlandite. bdl: below detection limit.

Sulfide type	Section	Lithology	<i>n</i>	Si	S	Fe	Co	Ni	Total	Ni/(Ni+Fe)
Pyrrhotite	1	A	3	0.1 (0.1)	46.4 (0.46)	52.8 (0.52)	bdl	0.8 (0.1)	100	0.01 (0)
Pyrrhotite	1	B	17	0.2 (0.2)	49.1 (2.6)	50.2 (2.8)	bdl	0.8 (0.4)	100	0.01 (0)
Pyrrhotite	1	C	7	0.4 (0.3)	48.1 (7.1)	47.9 (9.8)	0.7 (1.0)	3.5 (8.7)	100	0.10 (0.05)
Pyrrhotite	1	D	13	0.1 (0.2)	47.8 (1.5)	51.6 (1.5)	bdl	0.6 (0.1)	100	0.01 (0)
Intermediate	1	E								
Intermediate	2	A	6	0.4 (0.3)	47.1 (2.3)	45.8 (3.0)	0.3 (0.2)	6.3 (1.4)	100	0.12 (0.03)
Pyrrhotite	2	B	33	0.2 (0.2)	49.2 (2.3)	50.3 (2.4)	bdl	0.5 (0.1)	100	0.01 (0)
Pentlandite	2	C	1	0.1	44.9	27.1	1.4	26.6	100	0.50
Pyrrhotite	2	C	1	0.7	30.1	66.3	bdl	2.8	100	0.04
Intermediate	2	D	5	bdl	45.5 (0.8)	41.3 (8.0)	0.4 (0.3)	12.8 (8.4)	100	0.24 (0.10)
Pyrrhotite	2	D	2	bdl	46.6 (0.3)	52.5 (1.1)	bdl	1 (0.7)	100	0.02 (0.01)
Pentlandite	2	D	2	0.1 (0.2)	42.9 (0.9)	28.9 (2.5)	1.4 (0.1)	26.7 (3.3)	100	0.48 (0.04)
Pyrrhotite	2	E	3	bdl	51.4 (0.3)	48.3 (0.3)	bdl	0.4 (0.1)	100	0.01 (0)

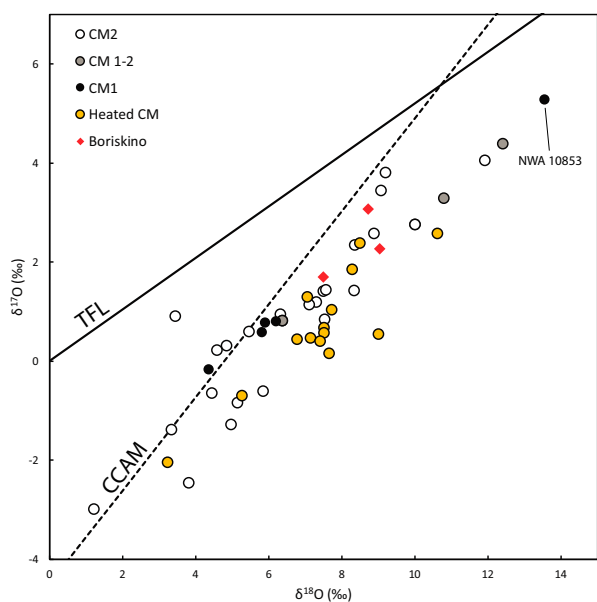


Fig. 8. Bulk O-isotopic composition of Boriskino (red diamonds). The terrestrial fractionation line (TFL) and carbonaceous chondrite anhydrous minerals mixing (CCAM) lines are plotted. CM are shown for comparison (Clayton et al. 1997; Clayton and Mayeda 1999; Irving et al. 2009; Howard et al. 2011; Hewins et al. 2014; Tonui et al. 2014; King et al. 2017; Meteoritical Bulletin Nos 96, 103, 105). (Color figure can be viewed at wileyonlinelibrary.com.)

in the $\delta^{17}\text{O}$ - $\delta^{18}\text{O}$ diagram would be expected and would digress from the bulk-carbonate-matrix (BMC) continuum reported in Verdier-Paoletti et al. (2017) that our measurements in Boriskino support.

Testing Hypotheses: Temperature Versus Water/Rock Ratio

The pseudomorphic replacement of chondrules by phyllosilicates (Fig. 4d) and the lack of anhydrous

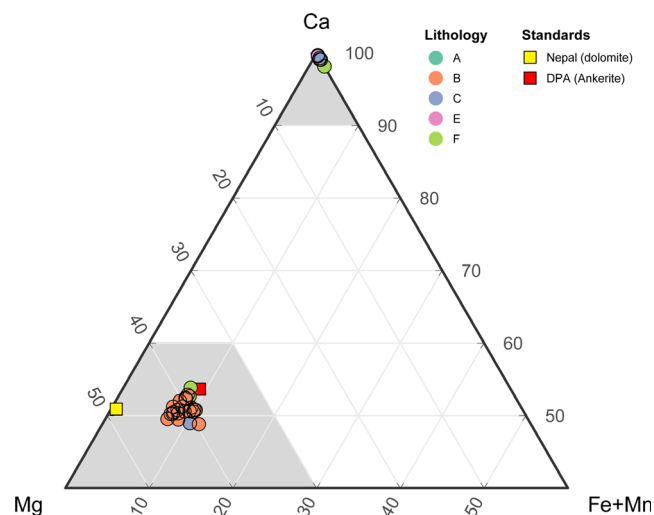


Fig. 9. Cropped Mg-Ca-(Fe+Mn) ternary diagram of carbonates (circles) in sections 3788-1 and 3788-2 (mole%) depending on host lithology. Calcite-aragonite and dolomite fields are represented as gray areas. The two available dolomite standards compositions (Nepal and DPA) are depicted by squares. Most carbonates have chemical compositions close to calcite or aragonite. Dolomite carbonates are ubiquitous in lithology B, whereas Ca-carbonates are absent. (Color figure can be viewed at wileyonlinelibrary.com.)

silicate minerals and metal in lithology B (Table 1) suggest that it experienced a higher degree of alteration than other clasts. This conclusion is consistent with the restricted occurrence of dolomites in lithology B, as dolomites are known to be exclusively present in heavily altered CM chondrites (Lee et al. 2014). Additionally, acicular sulfides have so far only been encountered in CM1 or CI clasts within breccias (e.g., Zolensky et al. 1996; Lindgren et al. 2013) and might therefore be restricted to heavily altered carbonaceous chondrites.

Table 3. Microprobe chemical analyses of Boriskino carbonates (mole%).

	Section	Lithology	Ca	Mg	Cr	Mn	Fe	S	Si	Ni	Sr	Na	Al	P	K	Fe+Mn	CaCO ₃ (wt%)	MgCO ₃ (wt%)
Nepal (dolomite)			50.9	48.3	–	0.1	0.8	–	–	–	–	–	–	–	–	0.8	52.9	42.3
DPA (ankerite)			51.6	35.9	–	0.3	12.2	–	–	–	–	–	–	–	–	12.5	52.4	30.7
cc1@1	2	A	98.0	0.7	–	–	0.4	0.3	0.6	–	–	–	–	–	–	0.4	99.7	0.6
cc1@1	1	A	98.5	–	–	–	0.4	–	–	–	–	–	–	1.1	–	0.4	98.9	–
cc1@2	1	A	98.3	–	–	–	0.4	–	–	–	0.3	–	–	1.0	–	0.4	96.5	–
cc3@2	1	A	97.9	–	–	–	0.7	–	–	–	0.3	–	–	0.9	–	0.7	97.2	–
cc3@3	1	A	97.5	–	–	–	0.8	–	–	–	0.3	–	–	1.0	–	0.8	97.2	–
dol3@1	2	B	49.7	38.5	–	2.8	8.5	–	0.5	–	–	–	–	–	–	11.3	50.7	33.1
dol4@1	2	B	50.3	41.4	–	1.4	6.9	–	–	–	–	–	–	–	–	8.3	52.2	36.1
dol5@2	2	B	50.4	40.3	–	2.2	6.7	–	0.4	–	–	–	–	–	–	8.9	50.6	34.1
dol7@1	2	B	50.6	38.9	–	3.4	6.7	–	0.4	–	–	–	–	–	–	10.1	50.6	32.8
dol8@1	2	B	51.1	39.4	–	1.6	7.9	–	–	–	–	–	–	–	–	9.5	52.2	33.9
dol8@2	2	B	50.0	41.3	–	1.8	6.6	–	0.4	–	–	–	–	–	–	8.4	51.9	36.1
dol9@1	2	B	52.4	39.4	–	3.0	5.1	–	–	–	–	–	–	–	–	8.1	53.8	34.0
dol9@2	2	B	51.2	41.5	–	2.2	5.0	–	–	–	–	–	–	–	–	7.2	52.4	35.8
dol6@1	1	B	48.9	41.3	–	1.7	7.0	–	–	–	–	0.7	–	0.5	–	8.7	50.3	35.8
dol7@1	1	B	50.5	41.0	–	3.6	4.4	–	–	–	–	–	–	0.5	–	8.0	52.0	35.5
dol7@2	1	B	50.3	41.7	–	2.9	4.7	–	–	–	–	–	–	0.4	–	7.7	52.8	36.8
dol8@2	1	B	50.0	42.1	–	1.8	5.6	–	–	–	–	–	–	0.5	–	7.4	52.3	37.0
dol9@1	1	B	50.0	41.8	–	2.8	4.9	–	–	–	–	–	–	0.5	–	7.7	51.6	36.3
dol9@2	1	B	49.8	39.2	–	3.1	6.2	0.7	0.4	–	–	–	–	0.5	–	9.4	49.3	32.7
dol9bis@1	1	B	48.3	39.3	–	2.4	9.0	0.5	–	–	–	–	–	0.4	–	11.4	50.0	34.1
dol9ter@1	1	B	49.3	42.8	–	2.8	4.6	–	–	–	–	–	–	0.4	–	7.4	51.1	37.3
dol10@1	1	B	52.6	38.8	–	3.2	5.0	–	–	–	–	–	–	0.4	–	8.1	54.8	34.0
dol10@2	1	B	52.1	39.2	–	3.2	5.0	–	–	–	–	–	–	0.5	–	8.2	52.3	33.2
dol16@2	1	C	48.6	40.4	–	4.9	5.4	0.3	–	–	–	–	–	0.4	–	10.3	49.4	34.5
cc12@1	1	C	97.8	–	–	–	0.7	–	–	–	–	0.6	–	0.9	–	0.7	100.3	–
cc12@2	1	C	98.4	–	–	–	0.7	–	–	–	–	–	–	0.9	–	0.7	97.7	–
cc5@1	1	E	98.7	–	–	–	0.3	–	–	–	–	–	–	1.0	–	0.3	99.1	–
cc5@2	1	E	98.8	–	–	–	0.3	–	–	–	–	–	–	0.9	–	0.3	98.3	–
cc3@1	2	F	96.5	–	–	–	1.8	1.2	0.5	–	–	–	–	–	–	1.8	96.9	–
cc3@2	2	F	99.6	–	–	–	0.4	–	–	–	–	–	–	–	–	0.4	100.3	–
dol11@1	2	F	50.7	40.0	–	4.4	3.9	–	1.1	–	–	–	–	–	–	8.3	52.0	34.5
dol11@2	2	F	52.7	38.8	–	4.5	3.9	–	–	–	–	–	–	–	–	8.5	53.2	33.0
dol11@3	2	F	53.8	38.2	–	3.8	4.3	–	–	–	–	–	–	–	–	8.1	55.4	33.1

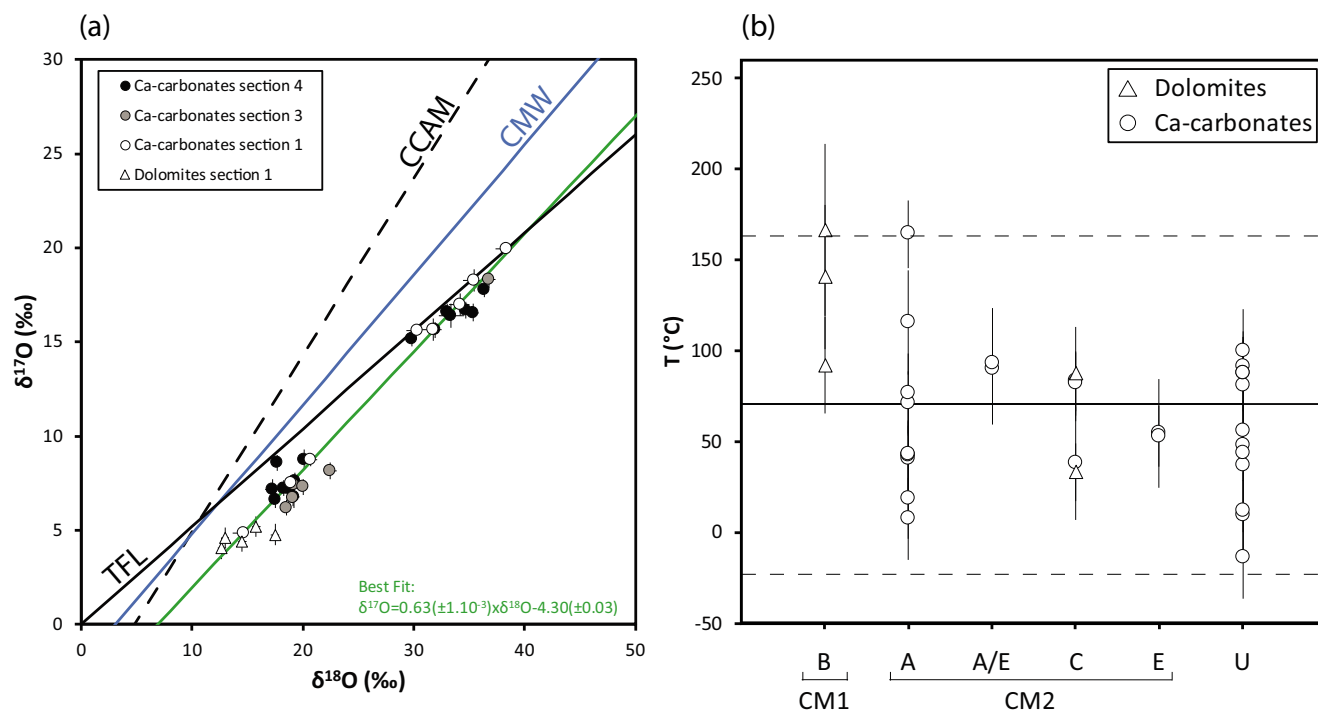


Fig. 10. a) Three-isotope plot of the O-isotopic compositions of Ca-carbonates and dolomite carbonates. Error bars are 2σ , but are often smaller than symbol. The X–Y-weighted best-fit regression of our measurements (following the calculations of York et al. (2004)) is displayed by the dashed green line. b) Precipitation temperatures of dolomites and Ca-carbonates separated by their respective lithology. U indicates carbonates hosted in undetermined lithologies. The average temperature ($70.3\text{ }^{\circ}\text{C}$) is shown by the continuous black line, and dashed black lines represent 2σ variations ($\pm 93.2\text{ }^{\circ}\text{C}$). (Color figure can be viewed at [wileyonlinelibrary.com](http://onlinelibrary.com).)

One exception is an occurrence in the CR chondrite LAP 02342, but the host regions were described as completely altered (Wasson and Rubin 2009). Together, these petrographic observations attest to two main types of clasts in Boriskino (1) CM1 clasts like lithology B and (2) CM2 clasts, for which the petrographic type cannot be determined precisely in this study. If those clasts originated from a single parent body, either a different thermal history or varying initial proportions of accreted ices might explain their apparently different degrees of alteration.

The parallel trends defined by the O-isotopic composition of Boriskino Ca-carbonates and those of other CM chondrites imply that their precipitation temperatures can be calculated following the procedure of Verdier-Paoletti et al. (2017). Applying this procedure yields a range of Ca-carbonate precipitation temperatures from -13.9 ± 22.4 to $164.2 \pm 18.6\text{ }^{\circ}\text{C}$, with an average of $60.3 \pm 74.0\text{ }^{\circ}\text{C}$ (2σ). This range of temperature is consistent with our previous study (Verdier-Paoletti et al. 2017). The negative temperatures recorded by a few carbonates account for a salt-rich water, such as brines, which below $0\text{ }^{\circ}\text{C}$ eutectic temperatures

allow for the presence of liquid water in the observed range of temperatures (e.g., Brass 1980; Oakes et al. 1990). This is consistent with the minor and trace element contents in carbonates of CM chondrites reported by Riciputi et al. (1994) accounting to a precipitation from a brine-like fluid, and the melting of a fluid inclusion in a halite crystal observed between -40 and $-35\text{ }^{\circ}\text{C}$ (Zolensky et al. 1999).

Dolomites plot on the same trend as Ca-carbonates. Consequently, the O-isotopic composition of the water from which they precipitated (δ_{water}) can also be retrieved, allowing the calculation of their precipitation temperatures using an adequate fractionation factor between dolomite and water ($10^3 \ln \alpha_{\text{dolomite/water}}^{\text{dolomite}} \approx \delta_{\text{dolomite}} - \delta_{\text{water}} = 3.140(\pm 0.022) \cdot \frac{10^6}{T^2} - 3.14(\pm 0.11)$; Horita 2014):

$$T_{\text{dolomite}}(\text{K}) = 10^3 \sqrt{\frac{3.140}{(\delta_{\text{dolomite}} - \delta_{\text{water}}) + 3.14}} \quad (1)$$

From our calculations, dolomite carbonates formed under similar conditions as Ca-carbonates, with precipitation temperatures ranging from 32.8 ± 16.1 to

Table 4. O-isotopic compositions of Ca-carbonates in Boriskino sections 3788-1/3/4.

Grain/measurement numbers	Section	Lithology	$\delta^{18}\text{O}$ (‰)	2 σ	$\delta^{17}\text{O}$ (‰)	2 σ	$\Delta^{17}\text{O}$	2 σ
cc12-1	1	C	34.2	0.8	17.0	0.6	-0.8	0.3
cc13-1	1	C	18.9	0.5	7.5	0.3	-2.3	0.1
cc13-2	1	C	20.7	0.5	8.7	0.3	-2.0	0.1
cc5-1	1	E	35.5	0.8	18.3	0.6	-0.2	0.3
cc5-3	1	E	31.7	0.5	15.6	0.3	-0.9	0.1
cc3-1	1	A/E	30.4	0.8	15.6	0.6	-0.2	0.3
cc4-1	1	A/E	14.7	0.8	4.8	0.6	-2.8	0.3
cc1-1	1	A	38.4	0.9	20.0	0.6	0.0	0.3
cc1-2*	3	A	18.5	0.3	6.2	0.4	-3.4	0.3
cc3-1*	3	A	19.1	0.4	6.7	0.4	-3.3	0.3
cc5-1*	3	A	19.2	0.4	7.4	0.4	-2.6	0.3
cc6-1*	3	A	22.5	0.6	8.2	0.4	-3.5	0.4
cc7-1*	3	A	20.0	0.4	7.3	0.4	-3.1	0.3
cc10-1*	3	A	36.8	0.6	18.3	0.4	-0.8	0.3
cc8-1*	4	A	17.2	0.7	7.1	0.6	-1.8	0.5
cc8-2*	4	A	17.6	0.2	8.6	0.4	-0.6	0.3
cc9-1*	4	A	19.3	0.5	7.6	0.4	-2.4	0.3
cc3-1*	4	Undetermined	33.0	0.5	16.6	0.4	-0.6	0.3
cc4-1*	4	Undetermined	36.3	0.5	17.8	0.4	-1.1	0.3
cc5-1*	4	Undetermined	31.9	0.3	15.6	0.4	-0.9	0.3
cc6-1*	4	Undetermined	33.4	1.1	16.4	0.6	-1.0	0.6
cc7-1*	4	Undetermined	34.7	0.5	16.7	0.4	-1.3	0.3
cc10-1*	4	Undetermined	18.6	0.6	7.2	0.5	-2.4	0.4
cc11-1*	4	Undetermined	20.1	0.2	8.8	0.5	-1.7	0.4
cc12-1*	4	Undetermined	19.2	0.5	6.8	0.6	-3.2	0.5
cc14-1*	4	Undetermined	18.2	0.3	7.2	0.4	-2.2	0.3
cc15-1*	4	Undetermined	35.4	0.5	16.6	0.5	-1.8	0.4
cc15-2*	4	Undetermined	29.8	0.4	15.2	0.4	-0.4	0.3
cc16-1*	4	Undetermined	17.5	0.3	6.6	0.5	-2.5	0.4

*Measurements from Vacher et al. (2018).

Table 5. O-isotopic compositions of dolomite-like carbonates in Boriskino section 3788-1.

Grain/measurement numbers	Section	Lithology	$\delta^{18}\text{O}$ (‰)	2 σ	$\delta^{17}\text{O}$ (‰)	2 σ	$\Delta^{17}\text{O}$	2 σ
dol9-2	1	B	12.7	0.4	4.0	0.6	-2.5	0.4
dol9-3	1	B	13.0	0.4	4.6	0.6	-2.1	0.4
dol10-1	1	B	14.5	0.4	4.4	0.5	-3.1	0.4
dol16-2	1	C	15.8	0.4	5.2	0.5	-3.0	0.4
dol16-3	1	C	17.5	0.4	4.8	0.6	-4.3	0.4

166.5 ± 47.3 °C (2 σ). Therefore, no clear distinctions in temperature ranges can be identified between lithologies (Fig. 10b). In detail, the same range of aqueous alteration temperatures for CM1 and CM2 lithologies suggests that temperature is not the controlling parameter of the degree of alteration. However, it is important to specify that carbonate precipitation temperature might not reflect the complete alteration thermal history, and therefore, caution has to be taken when interpreting those data. Nonetheless, O-isotopes in carbonates suggest a common thermal

history to all CM chondrites (Verdier-Paoletti et al. 2017). Therefore, it appears reasonable to assume that the CM1 and the CM2 lithologies experienced the same range of temperatures, and that a significant difference in temperature would at least have been preserved in the O-isotopic composition of a few carbonates if it existed. Consequently, we suggest that a higher water/rock ratio in the CM1 lithology could be the key to the observed textural and mineralogical differences relative to CM2.

We estimated the water/rock ratios of the CM1 and CM2 lithologies using two different methodologies (Clayton and Mayeda 1999; Young et al. 1999). According to the formalism of Young et al. (1999), the water/rock ratio (W/R) can be calculated as:

$$\frac{W}{R} = \frac{\delta_r^f - \delta_r^i}{\delta_w^i - \delta_w^f} \quad (2)$$

where $\delta_{w,r}^i$ represents the initial O-isotopic compositions of the water and rock, and $\delta_{w,r}^f$ their final compositions. The O-isotopic composition of initial liquid (i.e., $\delta^{18}\text{O} = 30.3\text{‰}$; Clayton and Mayeda 1984) is taken for δ_w^i , and that of anhydrous CM silicates (as a plausible CM protolith) for δ_r^i (i.e., $\delta^{18}\text{O} = -4.2\text{‰}$; Clayton and Mayeda 1999). We considered δ_w^f to be the lowest $\delta^{18}\text{O}_{\text{water}}$ in each lithology, calculated from the Ca-carbonate $\delta^{18}\text{O}$ values by connecting them to the CM water line along a mass-dependent line. This corresponds to a $\delta^{18}\text{O}$ value of $-8.2 \pm 3.1\text{‰}$ (2σ) for Ca-carbonates in CM2 lithologies and $-12.9 \pm 3.5\text{‰}$ (2σ) for dolomites in the CM1 clast. The δ_r^f value for CM2 was considered to be the lightest bulk value of Boriskino, as it represents the lowest degree of interaction with a $^{17,18}\text{O}$ -rich fluid. Finally, the average of bulk CM1 values was taken as δ_r^f for the CM1 lithologies (i.e., $\delta^{18}\text{O} = 5.6 \pm 1.6\text{‰}$, 2σ ; King et al. 2017), as no bulk measurements have been conducted on isolated CM1 clasts of Boriskino. However, we excluded CM1 NWA 10853, as it exhibits a heavy O-isotopic composition that we interpret as the result of postalteration thermal metamorphism. Our calculations suggest water/rock ratios of 0.26 and 0.30 for the CM1 and CM2 lithologies, respectively. These estimations are in line with a recent report based on other CM chondrites (Marrocchi et al. 2018). We could not estimate the error on our calculations because errors were not reported for the δ_w^i and δ_r^i values extracted from previous studies.

Based on a mass balance calculation of the transformation of olivine into serpentine (Clayton and Mayeda 1999), we estimate water/rock ratios of the CM1 and CM2 lithologies as:

$$\frac{W}{R} = \frac{f(\delta_s^f - \delta_r^i) + 2/7\Delta_{\text{sw}}}{\delta_w^i + \Delta_{\text{sw}} - \delta_s^f}, \quad (3)$$

where f is the fraction of altered rock, δ_s^f is the O-isotopic composition of serpentine, and Δ_{sw} is the fractionation factor between serpentine and water ($\delta_s^f - \delta_w^i$). Regarding Boriskino, we assumed that (1) δ_w^i and δ_r^i were the same as described above (30.3 and -4.2‰ , respectively); (2) following Clayton and

Mayeda's (1999) procedure, the proportion of rock altered is $f = 0.814$ for the CM2 portion, corresponding to the amount of matrix averaged over all the CM2 lithologies; and (3) $f = 1$ for the CM1 lithology as no anhydrous minerals remain. As serpentines formed at an average temperature of 70 °C (Verdier-Paoletti et al. 2017), we assumed that they precipitated from the same water as the cc5-1 carbonate in section 3788-3 (Vacher et al. 2018), which precipitated at 71 °C (Table 4). Considering $\Delta_{\text{sw}} = 8\text{‰}$ at 70 °C , this yields $\delta_s^f = 12.7\text{‰}$. These calculations suggest water/rock ratios of 0.75 and 0.61 for the CM1 and CM2 lithologies, respectively. As above, we cannot estimate errors on these calculations because errors on individual parameters were not reported in the literature sources.

Results from Equation 2 (Young et al. 1999) are counterintuitive (the more altered CM1 lithology should have experienced a higher water/rock ratio), but are easily explained as they rely on final bulk values of the rock. As a consequence, the result depends on the bulk values chosen for the CM1 and CM2 lithologies. Because the various clasts in Boriskino preclude an assessment of the dominant lithology in one aliquot, the bulk CM2 value used in the calculation might not be representative of the average bulk value of CM2 lithologies. Equation 3 (Clayton and Mayeda 1999) provides results consistent with CM1 being enriched in water relative to CM2. This suggests a locally higher concentration of ice or liquid water that could either be accounted for by (1) variations in the material permeability due to compaction induced by the impact (Rubin 2012) or (2) heterogeneous accretion of water ice grains during the parent body formation. The latter is rarely considered, but water ice mantling grain surface is believed to promote coagulation processes and can significantly contribute to the formation of planetesimals (e.g., Wang et al. 2005; Ros and Johansen 2013). The different constituents of chondrites (fine-grained material, chondrules, refractory inclusions, metal, etc.) do not have the same surface to volume ratios. Therefore, depending on the material and volume, the amount of ice might significantly change. This results in different amounts of ice being available at the hundreds of microns scale within chondrites, which show a heterogeneous distribution of those constituents at this scale.

Relative Chronology of Events

In CM chondrites, it is common to observe different extents of aqueous alteration between two clasts in a single sample, with no clear boundary between them (e.g., the Paris CM chondrite; Marrocchi et al. 2014; Vacher et al. 2017). As a result, it is often challenging to assess the relative chronology of

brecciation and aqueous alteration. Here, carbonate precipitation occurred in similar temperature ranges in all considered clasts, suggesting their concomitant alteration. Such conditions could be encountered both in primordial parent bodies and in a secondary body formed after brecciation. Yet, in the case of Boriskino, clast contacts are well defined at the macro- and microscopic scale (Figs. 1 and 2). During a postbrecciation alteration event, fluid flow and dissolution–precipitation processes would have obscured clast boundaries, which is not observed here. We note that this does not necessarily imply homogenization to the degree of aqueous alteration, as it has been shown that hydration can proceed in microenvironments of a few hundred microns (Brearley 2006; Bland et al. 2009).

The flattening of phyllosilicates and TCI clumps near clast boundaries (Fig. 6) strongly supports the idea of brecciation occurring after their formation. The same feature was reported in LON 94101 (Lindgren et al. 2013), therefore strengthening the idea of a main alteration event occurring before disruption of the parent body. Furthermore, several fractures cross multiple clasts at the macroscopic (Fig. 1) and microscopic scale (Figs. 2 and 3). Although these fractures would have favored fluid circulation, none are cemented with carbonates or other secondary minerals nor can any carbonate-filled veins be distinguished in elemental composite maps in this study. The absence of secondary minerals filling millimeter- to centimeter-sized fractures in Boriskino indicates that fragmentation of the parent body and agglomeration of debris occurred after aqueous alteration ended. However, this does not preclude the possibility that those cracks occurred upon the meteorite's fall to Earth; since Boriskino was recovered quickly after its fall was observed (Mason 1963), it is possible that its exposure to Earth's climate was too short to allow secondary minerals to cement in those cracks, but even evaporates can form during museum curation (Gounelle and Zolensky 2001). Nonetheless, we note that Vacher et al. (2018) reported the occurrence of one carbonate-filled vein in another section of Boriskino. Its light O-isotopic composition is consistent with a late precipitation event from an isotopically evolved fluid but preclude a terrestrial origin. However, cracks cemented with secondary minerals remain a scarce feature in Boriskino; only one has been reported in one of four different sections of the chondrite. Subsequent alteration events following brecciation may have remained local (hundreds of microns) and did not contribute significantly to the global textural and chemical modification of the chondrite.

SUMMARY

We conducted a petrographic, chemical, and isotopic study of the Boriskino CM breccia. Petrographic observations reveal an agglomeration of subcentimeter-size to centimeter-size clasts of differing lithologies with sharp boundaries visible at both the macro- and microscopic scales. Textural and mineralogical observations of each lithology are consistent with Boriskino being mainly composed of CM2 clasts. However, the chemical compositions of TCIs and the modal abundances of constituents in those regions were not sufficient to precisely determine their petrologic subtype following the procedure of Rubin et al. (2007). Nonetheless, one specific region exhibits a higher degree of alteration, identified as a CM1 degree owing to its lack of anhydrous minerals and the occurrence of dolomite carbonates and acicular iron sulfides. In addition, TCI and matrix phyllosilicates near the boundaries of these regions exhibit a strong foliation. These secondary phase deformations in areas where stresses should have been highest during reaccretion strongly suggest that brecciation occurred after aqueous alteration.

Our measurements of the O-isotopic compositions of Ca-carbonates and dolomites enable the determination of their precipitation temperatures following the procedure of Verdier-Paoletti et al. (2017). All carbonates, including those in the CM1 lithology, precipitated in similar temperature ranges between -14 ± 22 (2σ) and 167 ± 47 °C. Thus, no clear distinction can be drawn between CM1 and CM2 lithologies based on carbonate precipitation temperatures, suggesting that, in the case of Boriskino, temperature might not be the controlling parameter of the extent of aqueous alteration. However, according to our estimations for the CM1 and CM2 lithologies, the water/rock ratio could determine the extent of aqueous alteration in CM chondrites, even though it remains unclear if the small difference in water/rock ratio for the CM1 and CM2 lithologies could account for the observed textural and mineralogical differences. The duration of the rock's exposure to the alteration fluid likely plays a major role in the aqueous alteration extent; estimation of carbonate ages in the CM1 and CM2 lithologies using the ^{53}Mn - ^{53}Cr radiochronometer would clarify this hypothesis.

Last, our observations do not enable us to determine the origins of the different clasts. Indeed, our estimated ranges of carbonate precipitation temperatures could have been encountered either in a single parent body where geochemical conditions varied spatially or in multiple precursor parent bodies with specific geological histories. However, if the different extents of aqueous alteration are determined by local

variations in the water/rock ratio, then the various clasts could have originated from a single parent body. This could be easily explained by a heterogeneous distribution of liquid water during alteration either due to water being trapped in low permeability regions of the parent body or to variable amounts of ice available locally before the process. Otherwise, multiple precursors are required to explain the apparent diversity of aqueous alteration in Boriskino clasts.

Acknowledgments—We thank the Muséum National d'Histoire Naturelle of Paris for its loan of the four sections of Boriskino studied here: 3788-1/2/3/4. We thank Sylvain Pont and Isabella Pignatelli for their valuable insights on acicular sulfides. We thank Martin Lee and Alan Rubin for their constructive comments and associate editor Timothy Jull for careful editing. This work was funded by l'Agence Nationale de la Recherche through Grant ANR-14-CE33-0002-01 SAPINS (PI Yves Marrocchi). This is SAPINS contribution #12.

Editorial Handling—Dr. A. J. Timothy Jull

REFERENCES

- Bekaert D. V., Marrocchi Y., Meshik A., Remusat L., and Marty B. 2019. Primordial heavy noble gases in the pristine Paris carbonaceous chondrite. *Meteoritics & Planetary Science* 54:395–414.
- Benedix G. K., Leshin L. A., Farquhar J., Jackson T., and Thiemens M. H. 2003. Carbonates in CM2 chondrites: Constraints on alteration conditions from oxygen isotopic compositions and petrographic observations. *Geochimica et Cosmochimica Acta* 67:1577–1588.
- Bischoff A., Scott E. R. D., Metzler K., and Goodrich C. A. 2006. Nature and origins of meteoritic breccias. In *Meteorites and the early solar system II*, edited by Lauretta D. S. and McSween H. Y. Tucson, Arizona: The University of Arizona Press. pp. 679–712.
- Bland P. A., Jackson M. D., Coker R. F., Cohen B. A., Webber J. B. W., Lee M. R., Duffy C. M., Chater R. J., Ardakani M. G., and McPhail D. S. 2009. Why aqueous alteration in asteroids was isochemical: High porosity high permeability. *Earth and Planetary Science Letters* 287:559–568.
- Brass G. W. 1980. Stability of brines on Mars. *Icarus* 42: 20–28.
- Brearley A. J. 2006. The role of microchemical environments in the alteration of CM carbonaceous chondrites (abstract # 2074). 37th Annual Lunar Planetary Science Conference. CD-ROM.
- Briani G., Gounelle M., Bourot-Denise M., and Zolensky M. E. 2012. Xenoliths and microxenoliths in H chondrites: Sampling the zodiacal cloud in the asteroid Main Belt. *Meteoritics & Planetary Science* 47:880–902.
- Burbine T. H. 2014. Asteroids. In *Planets, asteroids, comets: The solar system*, edited by Davis A. M. Amsterdam: Elsevier. pp. 365–415.
- Chacko T. and Deines P. 2008. Theoretical calculation of oxygen isotope fractionation factors in carbonate systems. *Geochimica et Cosmochimica Acta* 72:3642–3660.
- Chizmadia L. J. and Brearley A. J. 2008. Mineralogy, aqueous alteration and primitive textural characteristics of fine-grained rims in the Y-791198 CM2 carbonaceous chondrite: TEM observations and comparison to ALHA81002. *Geochimica et Cosmochimica Acta* 72:602–625.
- Ciesla F. J., Lauretta D. S., Cohen B. A., and Hood L. L. 2003. A nebular origin for chondritic fine-grained phyllosilicates. *Science* 299:549–552.
- Clayton R. N. and Mayeda T. K. 1984. The oxygen isotope record in Murchison and other carbonaceous chondrites. *Earth and Planetary Science Letters* 67:151–161.
- Clayton R. N. and Mayeda T. K. 1999. Oxygen isotope studies of carbonaceous chondrites. *Geochimica et Cosmochimica Acta* 63:2089–2104.
- Clayton R. N., Mayeda T. K., Hiroi T., Zolensky M., and Lipschutz M. E. 1997. Oxygen isotopes in laboratory-heated CI and CM chondrites (abstract). *Meteoritics & Planetary Science* 32:A30.
- Davidson T. M., Ciesla F. J., and Collins G. S. 2012. Post-impact thermal evolution of porous planetesimals. *Geochimica et Cosmochimica Acta* 95:252–269.
- Fujiya W., Sugiura N., Marrocchi Y., Takahata N., Hoppe P., Shirai K., Sano Y., and Hiyagon H. 2015. Comprehensive study of carbon and oxygen isotopic compositions, trace element abundances, and cathodoluminescence intensities of calcite in the Murchison CM chondrite. *Geochimica et Cosmochimica Acta* 161:101–117.
- Gounelle M. and Zolensky M. E. 2001. A terrestrial origin for sulfate veins in CI1 chondrites. *Meteoritics & Planetary Science* 36:1321–1329.
- Gounelle M., Engrand C., Alard O., Bland P. A., Zolensky M. E., Russell S. S., and Duprat J. 2005. Hydrogen isotopic composition of water from fossil micrometeorites in howardites. *Geochimica et Cosmochimica Acta* 69:3431–3443.
- Greenwood R., Hutchison R., and Jones C. 1993. The structure and evolution of a CM2 regolith: A three-dimensional study of Cold Bokkeveld. *Meteoritics* 28:357–358.
- Gröning M. 2004. International stable isotope reference materials. In *Handbook of stable isotope analytical techniques*, vol. 1., edited by de Groot P. Amsterdam: Elsevier. pp. 874–906.
- Hanna R. D., Ketcham R. A., Zolensky M., and Behr W. M. 2015. Impact-induced brittle deformation, porosity loss, and aqueous alteration in the Murchison CM chondrite. *Geochimica et Cosmochimica Acta* 171:256–282.
- Hewins R. H., Bourot-Denise M., Zanda B., Leroux H., Barrat J., Humayun M., Göpel C., Greenwood R. C., Franchi I. A., and Pont S. 2014. The Paris meteorite, the least altered CM chondrite so far. *Geochimica et Cosmochimica Acta* 124:190–222.
- Heymann D. and Mazor E. 1967. Light-dark structure and rare gas content of the carbonaceous chondrite Nogoya. *Journal of Geophysical Research* 72:2704–2707.
- Horita J. 2014. Oxygen and carbon isotope fractionation in the system dolomite–water–CO₂ to elevated temperatures. *Geochimica et Cosmochimica Acta* 129:111–124.
- Howard K. T., Benedix G. K., Bland P. A., Gibson J., Greenwood R. C., Franchi I. A., and Cressey G. 2011.

- Mineralogical and O-isotope evolution in CM chondrites: On the non-relationship between bulk O-isotopes and degree of aqueous alteration (abstract #2429). 42nd Lunar and Planetary Science Conference. CD-ROM.
- Irving A. J., Kuehner S. M., Rumble D. III, Korotev R. L., and Clary S. 2009. Moapa Valley: A second non-Antarctic CM1 chondrite from Nevada, USA (abstract #5372). *Meteoritics & Planetary Science* 44:A96.
- King A. J., Schofield P. F., and Russell S. S. 2017. Type 1 aqueous alteration in CM carbonaceous chondrites: Implications for the evolution of water-rich asteroids. *Meteoritics & Planetary Science* 52:1197–1215.
- Lee M. R., Lindgren P., and Sofe M. R. 2014. Aragonite, breunnerite, calcite and dolomite in the CM carbonaceous chondrites: High fidelity recorders of progressive parent body aqueous alteration. *Geochimica et Cosmochimica Acta* 144:126–156.
- Lindgren P., Lee M. R., Sofe M. R., and Zolensky M. E. 2013. Clasts in the CM2 carbonaceous chondrite Lonewolf Nunataks 94101: Evidence for aqueous alteration prior to complex mixing. *Meteoritics & Planetary Science* 48:1074–1090.
- Lindgren P., Hanna R. D., Dobson K. J., Tomkinson T., and Lee M. R. 2015. The paradox between low shock-stage and evidence for compaction in CM carbonaceous chondrites explained by multiple low-intensity impacts. *Geochimica et Cosmochimica Acta* 148:159–178.
- Lindgren P., Lee M. R., Starkey N. A., and Franchi I. A. 2017. Fluid evolution in CM carbonaceous chondrites tracked through the oxygen isotopic compositions of carbonates. *Geochimica et Cosmochimica Acta* 204:240–251.
- Marrocchi Y., Gounelle M., Blanchard I., Caste F., and Kearsley A. T. 2014. The Paris CM chondrite: Secondary minerals and asteroidal processing. *Meteoritics & Planetary Science* 49:1232–1249.
- Marrocchi Y., Bekaert D. V., and Piani L. 2018. Origin and abundance of water in carbonaceous asteroids. *Earth and Planetary Science Letters* 482:23–32.
- Mason B. 1963. The carbonaceous chondrites. *Space Science Reviews* 1:621–646.
- McSween H. Y. 1979a. Are carbonaceous chondrites primitive or processed? A review. *Reviews of Geophysics* 17:1059–1078.
- McSween H. Y. 1979b. Alteration in CM carbonaceous chondrites inferred from modal and chemical variations in matrix. *Geochimica et Cosmochimica Acta* 43:1761–1770.
- Metzler K., Bischoff A., and Stöfler D. 1992. Accretionary dust mantles in CM chondrites: Evidence for solar nebula processes. *Geochimica et Cosmochimica Acta* 56:2873–2897.
- Nakamura T., Nagao K., Metzler K., and Takaoka N. 1999. Heterogeneous distribution of solar and cosmogenic noble gases in CM chondrites and implications for the formation of CM parent bodies. *Geochimica et Cosmochimica Acta* 63:257–273.
- Oakes C. S., Bodnar R. J., and Simonson J. M. 1990. The system NaCl- CaCl₂-H₂O: I. The ice liquidus at 1 atm total pressure. *Geochimica et Cosmochimica Acta* 54:603–610.
- Palmer E. E. and Lauretta D. S. 2011. Aqueous alteration of kamacite in CM chondrites. *Meteoritics & Planetary Science* 46:1587–1607.
- Pignatelli I., Marrocchi Y., Vacher L., Delon R., and Gounelle M. 2016. Multiple precursors of secondary mineralogical assemblages in CM chondrites. *Meteoritics & Planetary Science* 51:785–805.
- Pignatelli I., Marrocchi Y., Mugnaioli E., Bourdelle F., and Gounelle M. 2017. Mineralogical, crystallographic and redox features of the earliest stages of fluid alteration in CM chondrites. *Geochimica et Cosmochimica Acta* 209:106–122.
- Pignatelli I., Mugnaioli E., and Marrocchi Y. 2018. Cronstedtite polytypes in the Paris chondrite. *European Journal of Mineralogy* 30:349–354.
- Riciputi L. R., McSween H. Y., Johnson C. A., and Prinz M. 1994. Minor and trace element concentrations in carbonates of carbonaceous chondrites, and implications for the compositions of coexisting fluids. *Geochimica et Cosmochimica Acta* 58:1343–1351.
- Rollion-Bard C. and Marin-Carbonne J. 2011. Determination of SIMS matrix effects on oxygen isotopic compositions in carbonates. *Journal of Analytical Atomic Spectrometry* 26:1285–1289.
- Ros K. and Johansen A. 2013. Ice condensation as a planet formation mechanism. *Astronomy & Astrophysics* 552: A137.
- Rubin A. E. 2012. Collisional facilitation of aqueous alteration of CM and CV carbonaceous chondrites. *Geochimica et Cosmochimica Acta* 90:181–194.
- Rubin A. E. and Wasson J. T. 1986. Chondrules in the Murray CM2 meteorite and compositional differences between CM-CO and ordinary chondrite chondrules. *Geochimica et Cosmochimica Acta* 50:307–315.
- Rubin A. E., Trigo-Rodriguez J. M., Huber H., and Wasson J. T. 2007. Progressive aqueous alteration of CM carbonaceous chondrites. *Geochimica et Cosmochimica Acta* 71:2361–2382.
- Scott E. R., Keil K., and Stöfler D. 1992. Shock metamorphism of carbonaceous chondrites. *Geochimica et Cosmochimica Acta* 56:4281–4293.
- Tomeoka K. and Buseck P. R. 1985. Indicators of aqueous alteration in CM carbonaceous chondrites: Microtextures of a layered mineral containing Fe, S, O and Ni. *Geochimica et Cosmochimica Acta* 49:2149–2163.
- Tonui E., Zolensky M., Hiroi T., Nakamura T., Lipschutz M. E., Wang M. S., and Okudaira K. 2014. Petrographic, chemical and spectroscopic evidence for thermal metamorphism in carbonaceous chondrites I: CI and CM chondrites. *Geochimica et Cosmochimica Acta* 126:284–306.
- Tyra M. A., Farquhar J., Guan Y., and Leshin L. A. 2012. An oxygen isotope dichotomy in CM2 chondritic carbonates-A SIMS approach. *Geochimica et Cosmochimica Acta* 77:383–395.
- Vacher L. G., Marrocchi Y., Verdier-Paoletti M., Villeneuve J., and Gounelle M. 2016. Inward radial mixing of interstellar water ices in the solar protoplanetary disk. *The Astrophysical Journal Letters* 826:1–6.
- Vacher L. G., Marrocchi Y., Villeneuve J., Verdier-Paoletti M. J., and Gounelle M. 2017. Petrographic and C & O isotopic characteristics of the earliest stages of aqueous alteration of CM chondrites. *Geochimica et Cosmochimica Acta* 213:271–290.
- Vacher L. G., Marrocchi Y., Villeneuve J., Verdier-Paoletti M. J., and Gounelle M. 2018. Collisional and alteration history of the CM parent body. *Geochimica et Cosmochimica Acta* 239:213–234.
- Van der Plas L. and Tobi A. 1965. A chart for judging the reliability of point counting results. *American Journal of Science* 263:87–90.

- Van Kooten E. M. M. E., Cavalcante L. L., Nagashima K., Kasama T., Balogh Z. I., Peeters Z., Hsiao S. S.-Y., Shang H., Lee D.-C., Lee T., Krot A. N., and Bizzarro M. 2018. Isotope record of mineralogical changes in a spectrum of aqueously altered CM chondrites. *Geochimica et Cosmochimica Acta* 237:79–102.
- Verdier-Paoletti M. J., Marrocchi Y., Avicé G., Roskosz M., Gurenko A., and Gounelle M. 2017. Oxygen isotope constraints on the alteration temperatures of CM chondrites. *Earth and Planetary Science Letters* 458:273–281.
- Wang H., Bell R. C., Iedema M. J., Tsekouras A. A., and Cowin J. P. 2005. Sticky ice grains aid planet formation: Unusual properties of cryogenic water ice. *The Astrophysical Journal* 620:1027–1032.
- Wasson J. T. 1974. *Meteorites: Classification and properties*. Berlin: Springer-Verlag. 316 p.
- Wasson J. T. and Rubin A. E. 2009. Composition of matrix in the CR chondrite LAP 02342. *Geochimica et Cosmochimica Acta* 73:1436–1460.
- Wiik H. 1956. The chemical composition of some stony meteorites. *Geochimica et Cosmochimica Acta* 9:279–289.
- York D., Evensen N. M., Martinez M. L., and De Basabe Delgado J. 2004. Unified equations for the slope, intercept, and standard errors of the best straight line. *American Journal of Physics* 72:367–375.
- Young E. D., Ash R. D., England P., and Rumble D. 1999. Fluid flow in chondritic parent bodies: Deciphering the compositions of planetesimals. *Science* 286:1331–1335.
- Young E. D., Zhang K. K., and Schubert G. 2003. Conditions for pore water convection within carbonaceous chondrite parent bodies—Implications for planetesimal size and heat production. *Earth and Planetary Science Letters* 213:249–259.
- Zolensky M. E., Ivanov A. V., Yang S. V., Mittlefehldt D. W., and Ohsumi K. 1996. The Kaidun meteorite: Mineralogy of an unusual CM1 lithology. *Meteoritics & Planetary Science* 31:484–493.
- Zolensky M. E., Mittlefehldt D. W., Lipschutz M. E., Wang M., Clayton R. N., Mayeda T. K., Grady M. M., Pillinger C., and David B. 1997. CM chondrites exhibit the complete petrologic range from type 2 to 1. *Geochimica et Cosmochimica Acta* 61:5099–5115.
- Zolensky M. E., Bodnar R. J., Gibson E. K., Nyquist L. E., Reese Y., Shih C. Y., and Wiesmann H. 1999. Asteroidal water within fluid inclusion-bearing halite in an H5 chondrite, Monahans (1998). *Science* 285:1377–1379.

SUPPORTING INFORMATION

Additional supporting information may be found in the online version of this article:

Table S1. Chemical compositions (wt%) of bright and dark matrices in the different lithologies of sections 3788-1 and 3788-2.